Supporting information

Bamboo-like nitrogen-doped carbon supported chlorine-doped Fe_2P as an antibacterial oxygen reduction catalyst

Kai Cheng[a,b], Demin Jiang[a,b], Sainan Cai[a,b], Shikuo Li[c]*, Yuqiao Wang[a,b]*

[a] Research Center for Nano Photoelectrochemistry and Devices, School of Chemistry and Chemical Engineering, Southeast University, Nanjing 211189, China

[b] Yangtze River Delta Carbon Neutrality Strategy Development Institute, Southeast University, Nanjing 210096, China

[c] School of Material Science and Engineering, Anhui University, Hefei, 230601, China

*Corresponding author: Tel. & Fax +862552090621

E-mail: yqwang@seu.edu.cn (Y. Wang).

E-mail: lishikuo@ahu.edu.cn (S. Li).

Electrochemical measurements

Electrochemical measurements were conducted on CHI 760E workstation with a three-electrode system. The glassy carbon electrode was used as a working electrode, the Pt foil as a counter electrode and the Ag/AgCl as a reference electrode, respectively. All of potentials in electrochemical measurements were converted to the reversible hydrogen electrode (RHE) according to the following equation:

$$E_{RHE} = E_{\mathrm{Ag/AgCl}} + 0.059\mathrm{pH} + 0.197 \qquad (1)$$

The number of electrons transferred and HO_2^- production yield ($\%HO_2^-$) were accessed via the rotating ring-disk electrode (RRDE) mode. The number of electrons transferred and percentage peroxide formation were calculated according to the following equations:

$$n = 4 \times \frac{I_D}{I_D + I_R/N} \quad (2)$$

$$\%HO_2^- = 200 \times \frac{I_D/N}{I_D + I_R/N} \quad (3)$$

Here, I_D and I_R (mA cm^{-2}) are disk current and ring current, respectively. N represents the collection efficiency of the Pt ring (0.37).

Antibacterial activity

Escherichia coil (ATCC 25922) was selected as antibacterial model to conduct vitro antibacterial measurements. Luria bertani (LB) liquid medium and solid medium were prepared in advance for sterilization. Bacterial solution was diluted to 106 CFU/mL (CFU = colony-forming unit) with sterile phosphate buffered saline (PBS) solution, and then 0.1 mL dilute bacterial solution was inoculated on LB solid medium. 20 μL catalyst solution with the concentration of 0.1 g/mL was dropped on the 8 mm filter paper affixed on the medium. The blank control group was dropped the same volume of sterile water. The culture dish was placed in 37 ℃ incubator for 24 h. The antibacterial activity of the catalyst was characterized by measuring the diameter of the inhibition circle. The measurements were repeated three times to ensure the accuracy of the results. The results were colorized using the corresponding software for visualization.

Assembly and operation of MFCs

The air cathode was composed of catalyst layer, collector layer (100 mesh titanium mesh) and gas diffusion layer. 90 mg acetylene black and 150 μL 60% polytetrafluorethylene were sonicated for 30 min following by coating on one side of titanium mesh (3 cm × 3 cm) uniformly. The gas diffusion layer was obtained by heating it to 370 ℃ for 20 min, which contributed to the diffusion of O_2. Another side of the titanium mesh was coated with 4 mg cm^{-2} catalyst as catalyst layer for subsequent assembly. The anode was made by carbon cloth (2 cm × 3 cm) after pre-treatment. MFCs were operated with an external resistance of 1000 Ω at a constant temperature of 30 ℃. Anode electrolyte was renewed when the output voltage dropped below 50 mV. The electrolyte contained CH_3COONa (0.5 g L^{-1}), $NaH_2PO_4 \cdot 2H_2O$ (2.76 g L^{-1}), $Na_2HPO_4 \cdot 12H_2O$ (11.4 g L^{-1}), NH_4Cl (0.3 g L^{-1}) and KCl (1.3 g L^{-1}). The output voltage was recorded every 5 min through data acquisition instrument (USB-5936, Aertai,

China). Power density curves and polarization curves were measured by turning external resistors.

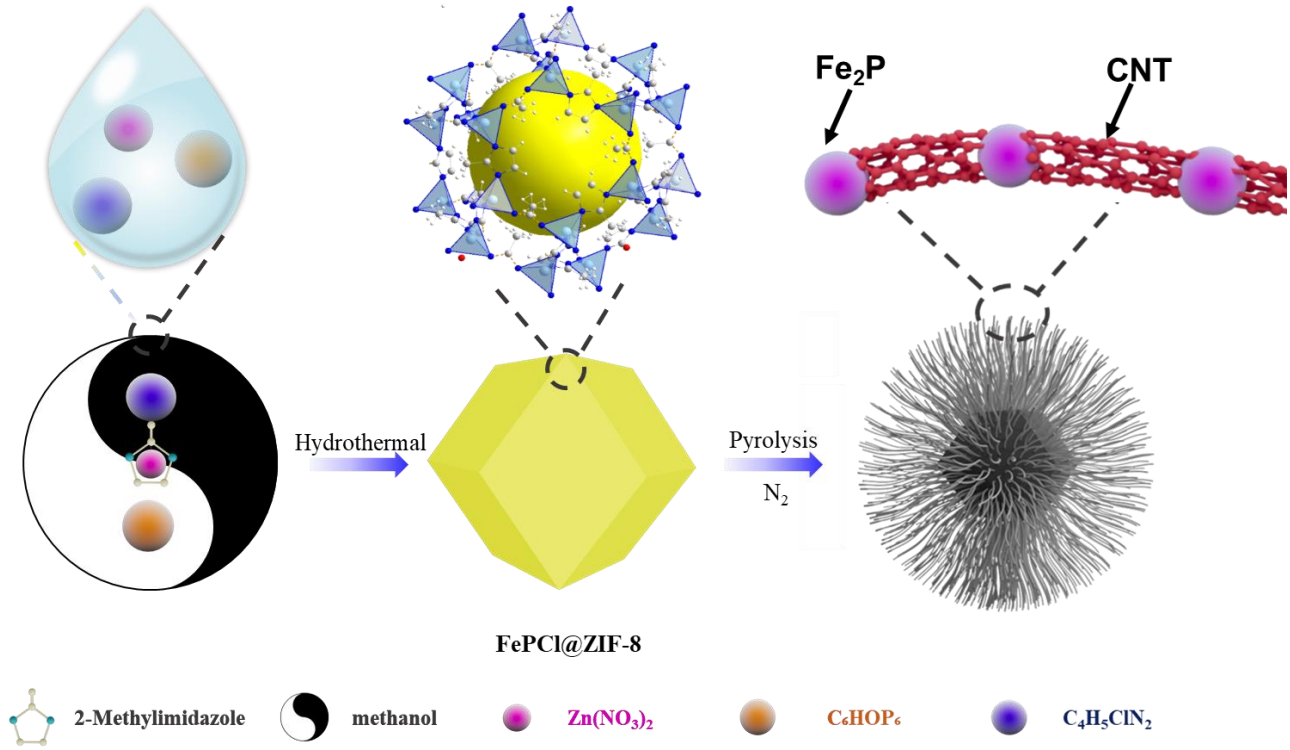

Figure S1. Schematic illustration for synthesis of Cl-Fe_2P/NC.

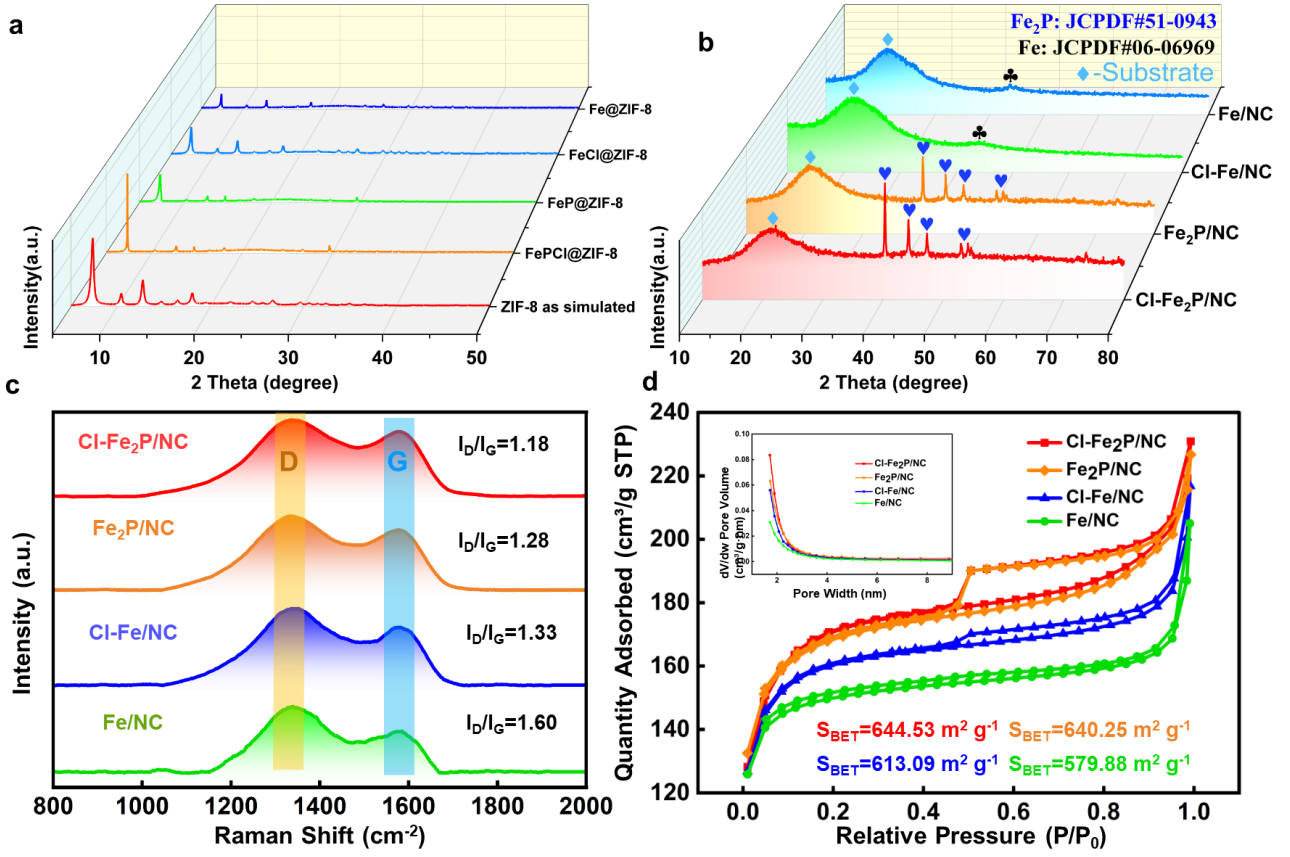

Figure S2 (a-b) XRD patterns. (c) Raman spectra. (d) N_2 adsorption–desorption isotherms and pore size distributions.

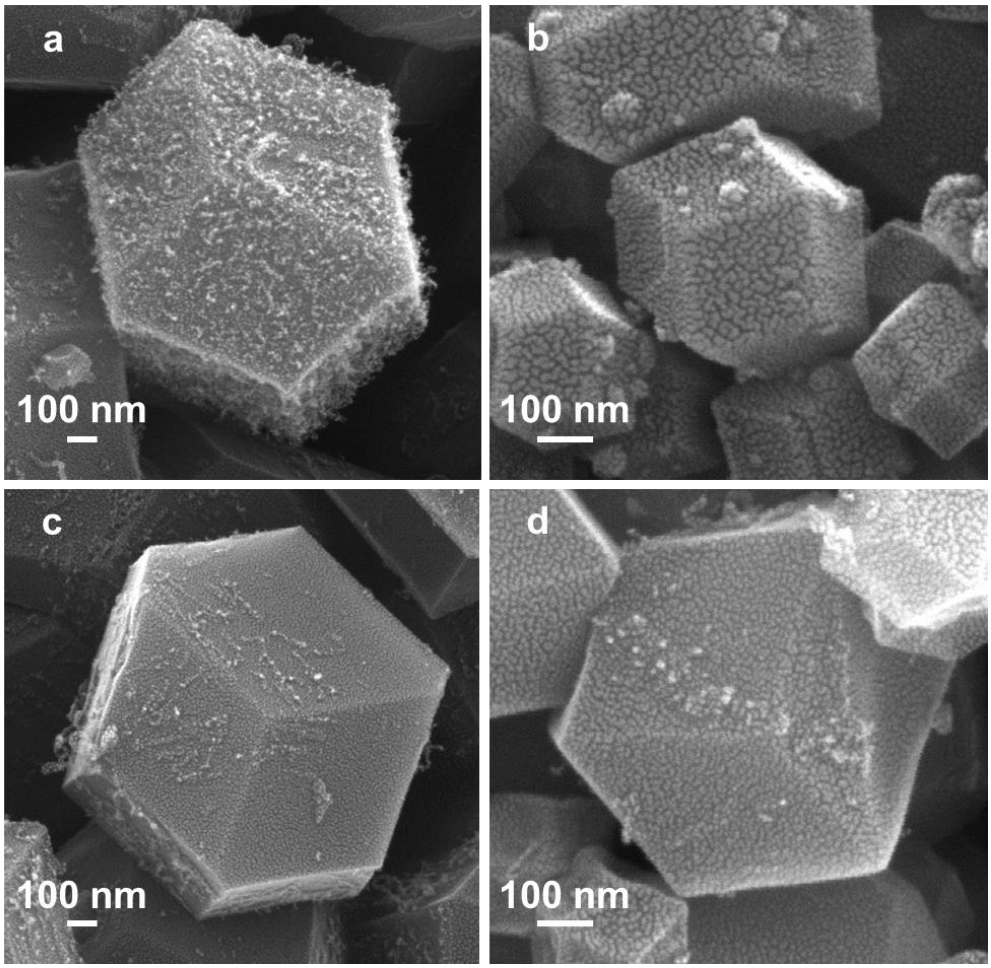

Figure S3. SEM images of (a) Cl-Fe_2P/NC, (b) Fe_2P/NC, (c) Cl-Fe/NC, (d) Fe/NC.

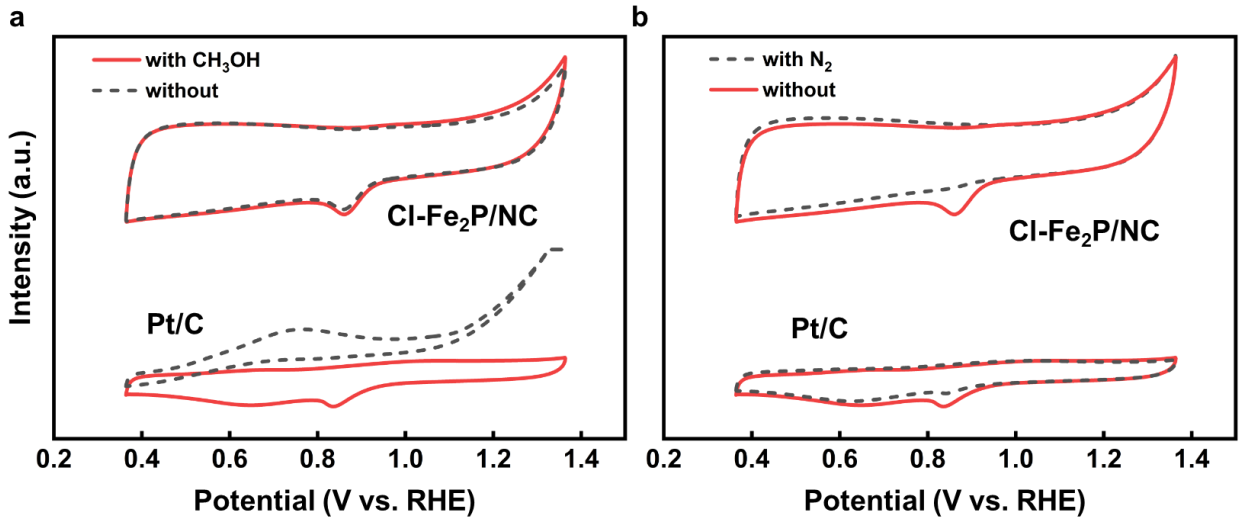

Figure S4. (a) CV curves in N_2-saturated 0.1 M KOH. (b) the resistance to poisoning of Cl-Fe_2P/NC and 20 wt% Pt/C.

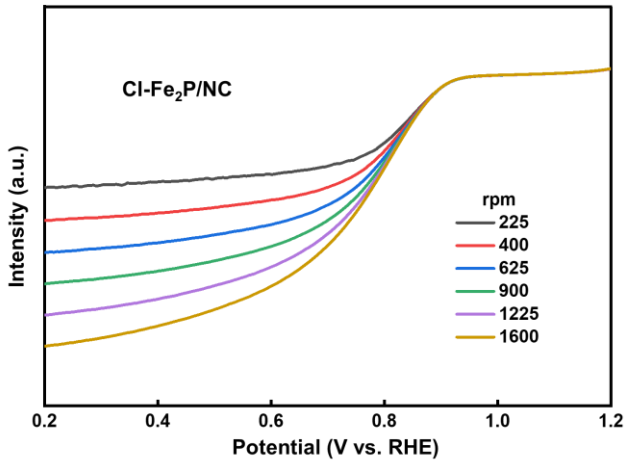

Figure S5. LSV with different electrode rotation speeds of Cl-Fe_2P/NC.

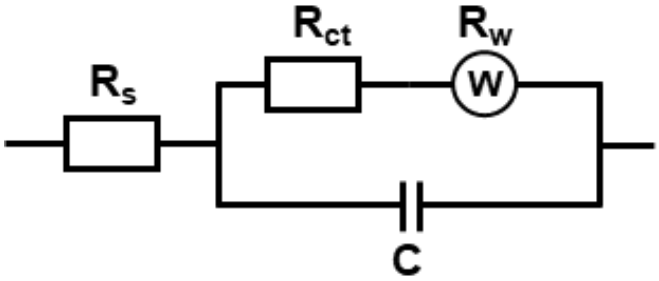

Figure S6. Equivalent circuit.

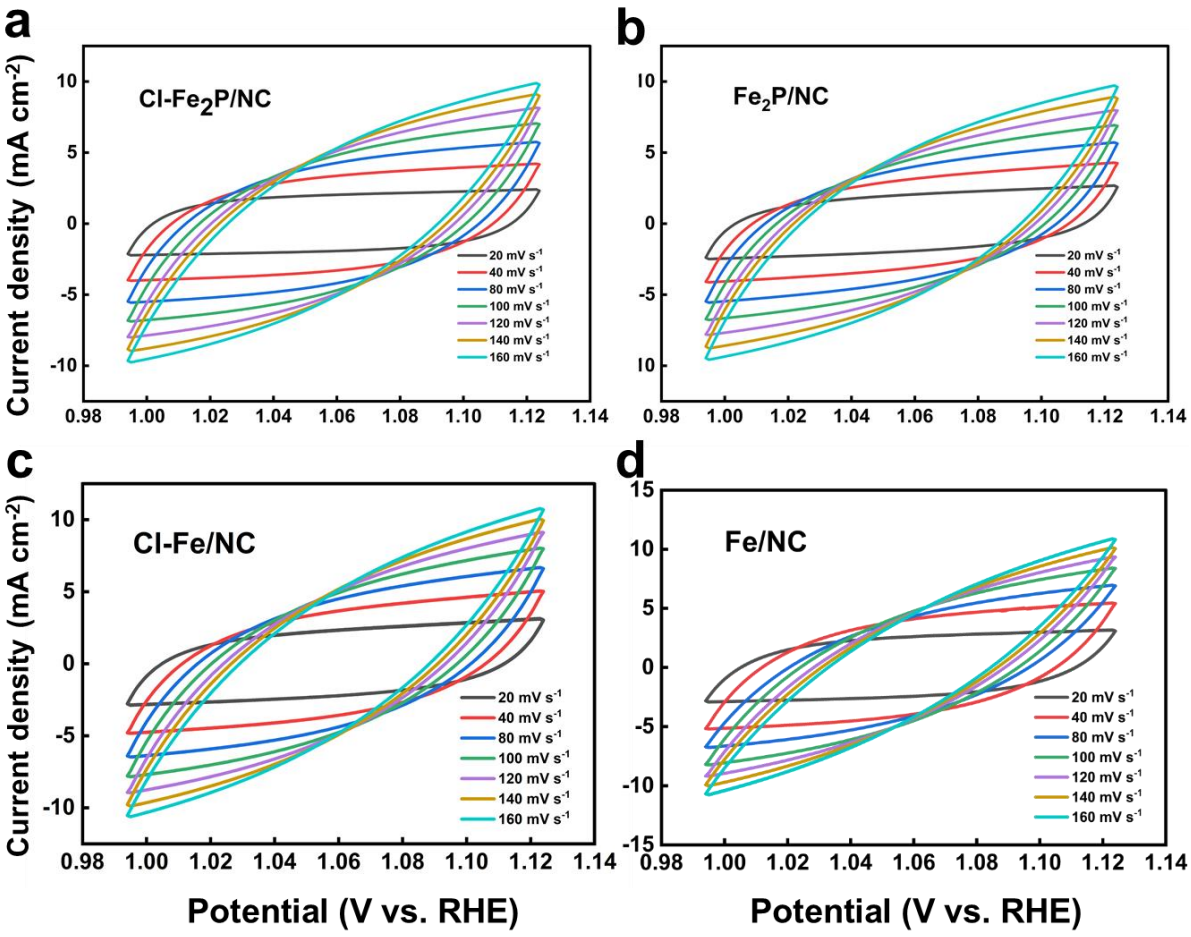

Figure S7. CV curves of (a) Cl-Fe_2P/NC, (b) Fe_2P/NC, (c) Cl-Fe/NC and (d) Fe/NC.

Table S1. Impedance fitting results

Catalysts	R_s (Ohm cm^{-2})	R_{ct} (Ohm cm^{-2})	R_w (Ohm cm^{-2})
Cl-Fe_2P/NC	0.62	0.50	0.81
Fe_2P/NC	0.67	0.49	0.88
Cl-Fe/NC	0.71	0.42	1.08
Fe/NC	0.83	0.21	1.09

Table S2. Summary of ORR activities of various catalysts in 0.1 M KOH.

Catalysts	Half-wave potential (V)	Onset potential (V)	Tafel slope (mV dec^{-1})	Ref.
Cl-Fe_2P/NC	**0.91**	**0.99**	**97.6**	**this work**
Pd−Gd_2O_3/C	0.877	0.986	55.5	1
FeSA-SeNC-meso/microporous	0.895	/	54.4	2
FeNPC	0.904	1.02	84	3
S-Zn-N-C-950	0.89	1.0	40.4	4
Fe_3O_4/La_2O_3@N,O-CNSs	0.88	1.05	40	5
Cu,Co/NSC1,	0.95	1.04	52.3	6
L_{10}-PtZn@N-C	0.93	1.04	67	7
Fe,$CoZn_{9+9}$-NO/WC	0.830	0.930	84.2	8

Table S3. The performance of air-cathode single-chamber MFCs equipped with the various ORR catalysts

Anode	Cathode	External Resistance	Output Voltage	Power Density	Ref.
Carbon cloth	**Cl-Fe_2P/NC**	**1000 Ω**	**600 mV**	**1505 mW m^{-2}**	**this work**
Carbon cloth	TiO2-NTs supported Co-Ni (1:1)	/	691 mV	104 mW m^{-2}	9
Carbon felt	MPC-800	1000 Ω	470 mV	240 mW m^{-2}	10
Carbon cloth	GCN–Co@CoO	1000 Ω	600 mV	611 mW m^{-2}	11
Carbon felt	GO/MgO	1000 Ω	401 mV	755.63 mW m^{-2}	12
Carbon cloth	Co/Al_2O_3-rGO	/	535 mV	548.19 mW m^{-2}	13
Carbon cloth	Cu/NC-700	/	553 mV	489.2 mW m^{-2}	14
Carbon cloth	NCA800	1000 Ω	/	1051mW m^{-2}	15
Carbon cloth	Cu-N/C@Cu-2	1000 Ω	503 mV	581 mW m^{-2}	16
Carbon cloth	C/$FeMnO_3$	1000 Ω	350 mV	460 mW m^{-2}	17
Carbon cloth	N-5-rGO@CNF	1000 Ω	622 mV	826 mW m^{-2}	18

References

1. S. Ning, M. Li, X. Wang, D. Zhang, B, Zhang, C. Wang, D. Sun, Y. Tang, H. Li, K. Sun, Importing Antibonding-Orbital Occupancy through Pd-O-Gd Bridge Promotes Electrocatalytic Oxygen Reduction. *Angew Chem Int Ed Engl,* 2023, **62**, e202314565.
2. T. He, X. Zhang, D. Li, Y. Qin, H. Zhao, Y. Wei, Y. Wang, S. Chen, S. Ding, C. Xiao, Hierarchical-Pore-Stabilization Strategy for Fabricating 18.3 wt% High-Loading Single-Atom Catalyst for Oxygen Reduction Reaction. *Small,* 2023, e2308530.
3. L. Fan, X. Wei, X. Li, Z. Liu, M. Li, S. Liu, Z. Kang, F. Dai, X. Lu and D. Sun, Phosphorus-doped iron-nitrogen-carbon catalyst with penta-coordinated single atom sites for efficient oxygen reduction, *Nano Res.*, 2022, **16**, 1810-1819.
4. Y. Tan, Z. Zhang, S. Chen, W. Wu, L. Yu, R. Chen, F. Guo, Z. Wang and N. Cheng, Local geometric distortion to stimulate oxygen reduction activity of atomically dispersed Zn‐Nx Sites for Zn–Air Batteries, *Adv. Funct. Mater.*, 2023, 2311337.
5. T. Li, L. Zhang, L. Zhang, J. Ke, T. Du, L. Zhang, Y. Cao, C. Yan and T. Qian, Tailoring the chemisorption manner of Fe d‐Band center with La_2O_3 for enhanced oxygen reduction in anion exchange membrane fuel cells, *Adv. Funct. Mater.*, 2023, 2309886.
6. Y. Chen, J. Mao, H. Zhou, L. Xing, S. Qiao, J. Yuan, B. Mei, Z. Wei, S. Zhao, Y. Tang and C. Liu, Coordination shell dependent activity of CuCo diatomic catalysts for oxygen reduction, oxygen evolution, and hydrogen evolution reaction, *Adv. Funct. Mater.*, 2023, 2311664.
7. S. Lu, Y. Hu, F. Xia, S. Yang, S. Jiang, Y. Zhou, D. Ma, W. Zhang, J. Li, J. Wu, D. Rao and Q. Yue, Simultaneously geometrical and electronic modulation of L(10) -PtZn by trace ge boosts high-performance oxygen reduction reaction, *Small*, 2023, e2305296.
8. J. Xue, Z. Liu, Y. Fan, R. Wang and Y. Li, ZIF-derived Fe,Co coordinated N/O-codoped three-dimensional tungsten–carbon matrix for the performance-enhanced zinc-air flow battery and water splitting, *Chem. Eng. J.*, 2023, **476**, 146502.
9. A. Chaturvedi, S. Dhillon and P. Kundu, 1-D semiconducting TiO_2 nanotubes supported efficient bimetallic Co-Ni cathode catalysts for power generation in single-chambered air-breathing microbial fuel cells, *Sustain. Energy Technol. Assess.*, 2022, **53**, 102479.

10. Z. Zha, Z. Zhang, P. Xiang, H. Zhu, X. Shi and S. Chen, Porous graphitic carbon from mangosteen peel as efficient electrocatalyst in microbial fuel cells, *Sci. Total Environ.*, 2021, **764**, 142918.
11. L. Tan, Q. Pan, X. Wu, N. Li, J. Song and Z. Liu, Core@Shelled Co/CoO embedded nitrogen-doped carbon nanosheets coupled graphene as efficient cathode catalysts for enhanced oxygen reduction reaction in microbial fuel cells, *ACS Sustain. Chem. Eng.*, 2019, **7**, 6335-6344.
12. W. Yang, G. Chata, Y. Zhang, Y. Peng, J. Lu, N. Wang, R. Mercado, J. Li and S. Chen, Graphene oxide-supported zinc cobalt oxides as effective cathode catalysts for microbial fuel cell: High catalytic activity and inhibition of biofilm formation, *Nano Energy*, 2019, **57**, 811-819.
13. F. Papiya, A. Nandy, S. Mondal and P. Kundu, Co/Al_2O_3-rGO nanocomposite as cathode electrocatalyst for superior oxygen reduction in microbial fuel cell applications: The effect of nanocomposite composition, *Electrochim. Acta*, 2017, **254**, 1-13.
14. S. Dhillon, A. Chaturvedi, D. Gupta, T. Nagaiah and P. Kundu, Copper nanoparticles embedded in polyaniline derived nitrogen-doped carbon as electrocatalyst for bio-energy generation in microbial fuel cells, *Environ. Sci. Pollut. Res. Int.*, 2022, **29**, 80787-80804.
15. W. Yang, Y. Peng, Y. Zhang, J. Lu, J. Li and S. Chen, Air cathode catalysts of microbial fuel cell by nitrogen-doped carbon aerogels, *ACS Sustain. Chem. Eng.*, 2018, **7**, 3917-3924.
16. B. Lai, H. Wei, Z. Luo, T. Zheng, Y. Lin, Z. Liu and N. Li, ZIF-8-derived Cu, N co-doped carbon as a bifunctional cathode catalyst for enhanced performance of microbial fuel cell, *Sci. Total Environ.*, 2023, **856**, 159083.
17. F. Shahbazi Farahani, B. Mecheri, M. R. Majidi, E. Placidi and A. D'Epifanio, Carbon-supported Fe/Mn-based perovskite-type oxides boost oxygen reduction in bioelectrochemical systems, *Carbon*, 2019, **145**, 716-724.
18. M. Xu, L. Wu, M. Zhu, Z. Wang, Z. Huang and M. Wang, Self-supporting nitrogen-doped reduced graphene oxide@carbon nanofiber hybrid membranes as high-performance integrated air cathodes in microbial fuel cells, *Carbon*, 2022, **193**, 242-257.